Tuning Film Stresses for Open-Air Processing of Stable Metal Halide Perovskites

Muneeza Ahmad[1], Carsen Cartledge[1], Gabriel McAndrews[2], Antonella Guiri[3], Michael D. McGehee[2], Aurora Rizzo[3], and Nicholas Rolston[1]*

1. Arizona State University, Tempe, AZ, 85281, USA

2. Materials Science and Engineering, University of Colorado, Boulder, Colorado 80309, United States

3. CNR NANOTEC - Institute of Nanotechnology c/o Campus Ecotekne, University of Salento, via Monteroni, I-73100 Lecce, Italy

Graphical Abstract:

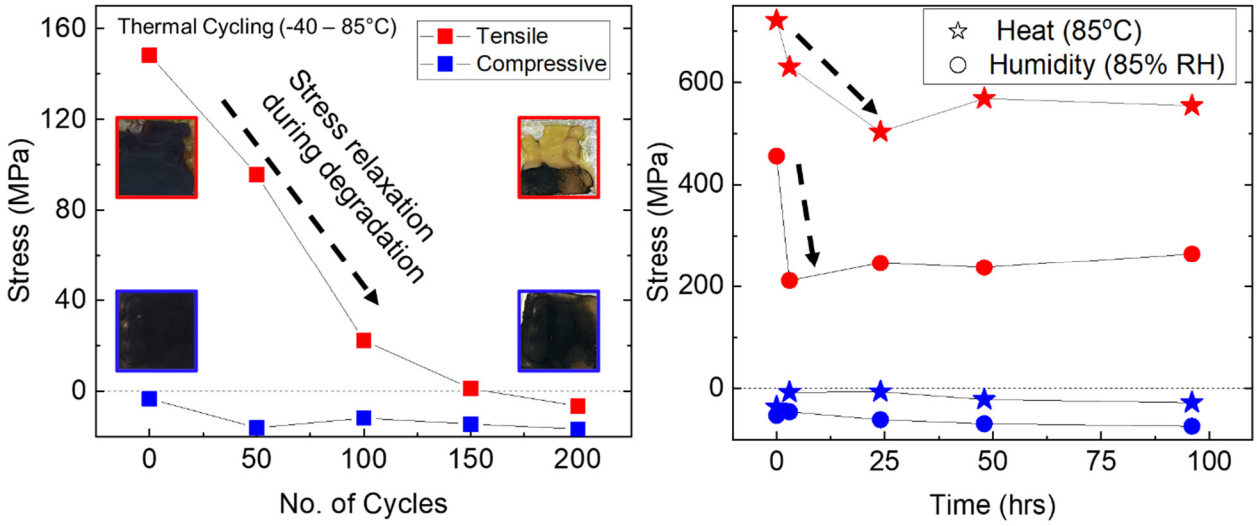

I. Introduction

Perovskite semiconductors are attractive for solar cells because they are defect-tolerant with long charge carrier lifetimes due to the lack of deep level trap states, and high carrier mobility [1]–[4]. These parameters make them a viable competitor to existing solar cell technologies, but they suffer from environmental and mechanical instabilities [5]–[8] . Mechanical film stress is a key challenge for perovskites and all thin film device technologies. Metal halide perovskites are brittle in nature, which facilitates crack propagation and undermines device reliability [9]. Above a critical value, biaxial stresses—whether they are residual or applied—lead to cracking along the brittle film plane and the perovskite layer is pulled off the substrate due to tensile stresses. [10]

Residual stresses, especially if they are tensile in nature, prove to be detrimental to the performance and stability of a perovskite solar cell. They are known to affect the bandgap, lead to structural instability, an increase in defect density, reduced carrier mobility, increased ionic mobility, higher risk of cracking or

mechanical failure and lower cell efficiency [11]–[14]. As shown in **Fig. 1 (a)**, an applied tensile stress can cause the perovskite film to break down into the yellow PbI_2 phase and create a path for rapid ion migration which might relieve some of the thermally induced stress. Stress relaxation is a common effect seen in different classes of materials and is ascribed to the breaking of bonds in metals [15] or the movement of polymer chains in elastic fibers [16]. Previous research on stress in perovskite solar cells has shown that tension leads to an increase in ion migration and accelerates breakdown of methylammonium lead iodide to lead iodide [17]. Compressive stresses, on the other hand, are desirable up to a certain critical value as they can heal structural defects such as dislocations and improve the stability of the perovskite thin films. Applying an external compressive stress can also mechanically treat the cracks in a perovskite film [18].

Large tensile residual stresses in a film can lead to delamination or fracture. It is important to look at the driving force for fracture, G in equation (1) using the film thickness t_f, Young Modulus of perovskite E, and numerical factor z which we assume to be 1.

$$G = \frac{z\sigma^2 t_f}{E} \quad (1)$$

Fracture will occur when $G > G_c$ where G_c is the critical driving force for fracture. We have previously observed that long-chain polymer additives such as starch can increase G_c of the perovskite, which would allow these modified films to withstand higher stresses without fracturing. [19] Our measured fracture energy for samples with these additives is approximately 5 J/m^2 and will be published in another work. **Fig. 1(c)** shows modeled G values along with experimental data, noting that in unmodified perovskite thin films, the critical driving force for fracture is around 1.5 J/m^2 based on previous experimental results. The fracture energy also heavily depends on the thickness of the film, and our measured thicknesses varied with the addition of polymers (Table S1, S2). Note that equation (1) is only valid for films under tensile stress because the failure mechanisms are different in compression, and therefore only films with residual tensile stress are shown in **Fig. 1 (c)**. Even though no visible fractures occurred in the samples after processing, the increase in *G* with tensile stress is expected to induce accelerated degradation as was shown above. This is because of synergistic effects of mechanical and environmental stressors leading to damage processes and degradation in the perovskite films.

Film stresses result from a combination of thermal, intrinsic, or epitaxial effects [20], although the latter is not applicable for solution-processed perovskites because of their polycrystalline structure. As such, stress in perovskites fabricated by solution-processing techniques will result from either thermal or intrinsic stresses. Thermal stresses usually originate because of the large coefficient of thermal expansion (CTE) mismatch between typically used stiff substrates and the perovskite thin film. Silica glass, silicon, and perovskite have approximate coefficients of thermal expansion of 5.0 x 10^{-6}/°K, 2.5 x 10^{-6}/°K and 50 x 10^{-6}/°K respectively [21][22]. This means that perovskites can expand or contract up to 10 times more than glass and 20 times more than silicon substrates. Once the perovskite has completely converted upon annealing, it cools down and shrinks but the substrate restricts it from contracting freely which leads to tensile stress. This CTE difference can lead to a change in stress of ~ 315 to 115 MPa for a highly tensile sample (residual stress of 250 MPa) and ~ 115 to -85 MPa for a compressive sample (residual stress of -20 MPa) as shown in **Fig 1 (b)** in a silicon/perovskite system when it is thermally cycled from -40 to 85°C. We used Equation 2 to calculate the thermal stresses where E_f is the Young's Modulus of the film, v_f is the Poissons's ratio for the film, α_s is the CTE of the substrate, α_f is the CTE of the film and $\triangle T$ is the change in temperature. There has been some work done on reducing the biaxial tensile stress by using substrates with a higher CTE [12], but that is not an option in the case of perovskite-silicon tandem solar cells.

$$\sigma_f = \left(\frac{E_f}{1-\nu_f}\right)(\alpha_s - \alpha_f) \triangle T \qquad (2)$$

The vast majority of perovskite processing has involved rapid crystallization through quenching (i.e.- antisolvent or gas) to dry and convert the precursor to an intermediate Lewis adduct phase. It is then converted into the final perovskite phase by annealing the film at temperatures of around 100°C. The residual stresses in the final film are therefore dominated almost entirely by thermal effects and efforts to model and understand the stress have focused on the use of equation 2. However, there are other intrinsic

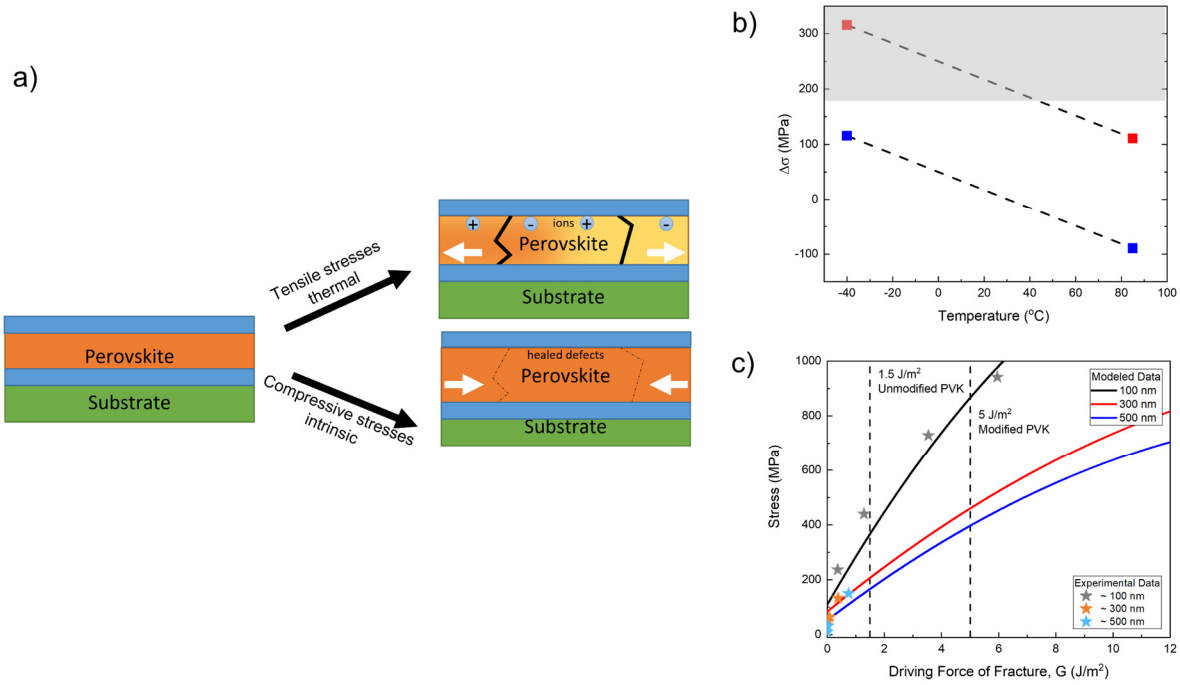

Fig 1 (a) Schematic demonstrating the effects of tensile thermal stresses on the perovskite film, leading to yellow PbI_2 phase, cracks and ion migration whereas compressive stresses heal defects. 1 (b) The changes in stress when a highly tensile and (c) compressive sample is subjected to thermal loads ranging from -40 to 85°C. The highlighted region is the stress at which fracture, or delamination would occur. c) Film stress vs. driving force for fracture, G, calculated for perovskite films with additives of different thicknesses. The reference line at 1.5 J/m^2 is the critical driving force above which fracture typically occurs (G_c) in unmodified perovskites and the line at 5 J/m^2 is for modified perovskites.

effects that need to be considered as well. Moreover, previous studies conducted on stress have used unscalable methods such as spin coating inside the glovebox. [12], [23]

Intrinsic stresses from factors such as dislocation density and grain boundaries could play a role in perovskite films. They originate during film growth and are determined by the crystallization and nucleation regime that is dominant during the process. Intrinsic stresses have been well-characterized and mapped to ionic deposition conditions in older solar cell technologies such as amorphous silicon [24]. However, there remains a knowledge gap when it comes to stress and its relationship with processing techniques, microscopic structure, and the macroscopic properties for thin film perovskites.

There have been some recent reports which have shown that additives can modify the stress state in perovskites is based on changing morphology, but the mechanism is not understood [25], [26]. Bulk

additives have been explored by several groups to reduce the tensile stress. The introduction of a polymer such as polyethylene glycol (PEG) [27] or polymethyl methacrylate (PMMA) [28] can slow down the crystallization process and help improve film morphology. These polymer additives form heterogenous nucleation sites for perovskites that promote crystal growth in a preferred orientation. It is therefore possible to improve mechanical integrity through stress reduction and maintain desirable film growth without changing the composition or bandgap of the perovskite. A fundamental understanding of the mechanism for film stress as it relates to morphology of perovskite layers is therefore required to achieve mechanical stability in full devices [29].

We hypothesize that different processing routes can be used to control the intrinsic stress and the final stress state of the film depending on how solvent is removed. We compare the effects of both spin coating and blade coating on film stresses and how they are driven by polymer additives. Both the spin coating and blade coating techniques remove the antisolvent application step and eliminate quenching. Our blade coating process is not only suited for large-area deposition but is also performed in an open-air environment which further improves scalability. In this work, we also introduce rheological modifiers—food additives and thickening agents commonly known as gellan gum and corn starch—to the precursor solution to study the effects of biopolymers on the residual stress of perovskite thin films. After demonstrating control over the residual film stress, we show that the optoelectronic properties and film stability are markedly improved through compressive stress engineering. Our work involves a systematic study of the processing to identify the conditions that lead to intrinsic stresses with the goal of understanding how to induce desirable compression in the perovskite film with the help of biopolymer additives.

II. Results and Discussion

We introduced biopolymer additives, either corn starch or gellan gum, to the precursor solution to slow down the crystallization and tune corresponding morphology of the perovskite film using spin coating or blade coating without the use of antisolvent. The use of non-toxic biopolymers to achieve thermal stability was not only motivated by their assistance with the crystallization of the perovskite but also their effect on the free energy of nucleation and growth, and improvements in fracture energy [19], [30]–[32]. **Fig. 2 (a)** shows the surface profile of the perovskite thin film without any additives from blade coating in open-air. The resultant film (**Fig, 2 (b)**) is rough with gaps and rapid nucleation of the perovskite solution evident by the needle-shaped crystals attributed to the PbI_2 phase of perovskite [33]. Addition of biopolymers helps create a relatively smooth and uniform film without the need for any

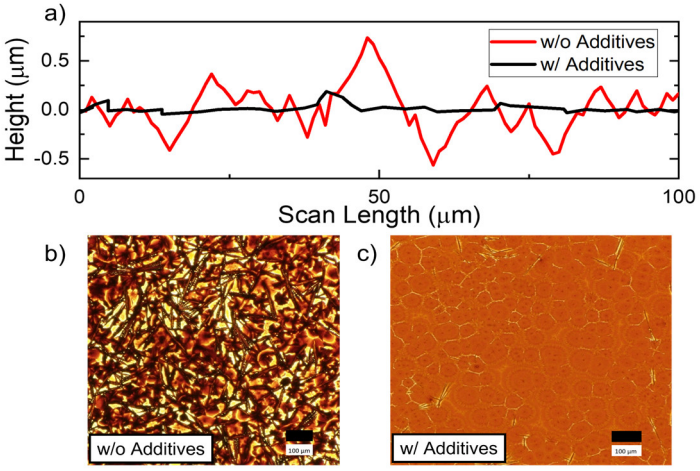

Fig 2 (a) The surface profile of the $MAPbI_3$ thin film with and without additives. The surface morphology as seen in optical transmission microscope images (b) blade coating without additives and (c) blade coating with additives is also shown.

quenching. The crystallization slows down because of a more viscous precursor solution achieved with the additives as shown in **Fig S2**. Biopolymers can also overcome the the activation energy for nucleation [22] and help maintain a balance between nucleation and growth regimes during film solidification which enables an improved morphology with a decrease in the average surface roughness from 138 nm to 35 nm. Uncontrolled transformation from the solution phase to the solid phase without quenching can lead to incomplete conversion of the perovskite, non-uniformity of the grains, and more grain boundaries or point defects in the absorber layer. A uniform and high-quality film is important for achieving high conversion efficiencies [34]. With the introduction of additives, we achieved better coverage of the perovskite thin

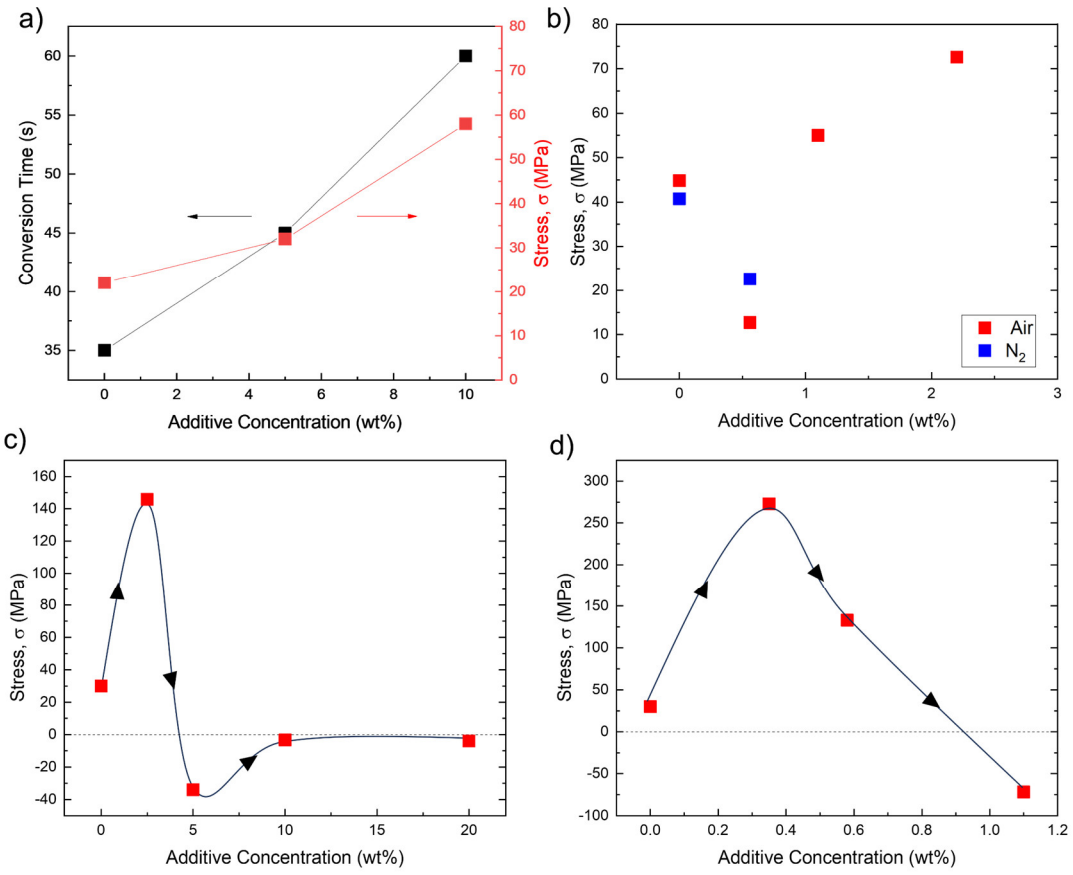

Fig 3 (a) The conversion time and measured film stress for spin coated samples with corn starch and (b) stress for gellan gum spun in N_2 and air (40% RH) and blade coated samples with (c) corn starch and (d) gellan gum in terms of the concentration of each additive in the perovskite precursor.

films with more homogenous domains and a more uniform thickness.

Previous work has shown an improved photovoltaic performance for $MAPbI_3$ devices with the addition of the starch polymer. The power conversion efficiency for the best device with 10wt% starch was 18.8% with a V_{OC} of 1.10 V, J_{SC} of 21.9 mA/cm^2 and a fill factor of 78.3%. This was much higher than their best perovskite-control device which had a power conversion efficiency of 17.0% with a V_{OC} of 1.09 V, J_{SC} of 20.5 mA/cm^2 and a fill factor of 75.5% [19]. The high quality film due to polymer-assisted crystallization helps achieve higher solar cell efficiencies.

We measured residual stress using a laser scanning curvature-based measurement tool. **Fig. S1** shows the curvature of the silicon substrate before and after deposition of the perovskite thin film. The film stress is calculated using the Stoney's equation given below in equation (3), where E and v are the Young's Modulus and Poisson's ratio for the substrate, t_s is the substrate thickness and t_f is the film thickness and $\triangle\kappa$ is the change in curvature. This quick and non-destructive measurement technique allows for the quantification of residual film stresses and their changes over time.

$$\sigma_f = \left(\frac{E}{1-v}\right)_s \frac{t_s^2}{6t_f} \triangle \kappa \qquad (3)$$

Methylammonium lead iodide ($MAPbI_3$) perovskite films processed through spin coating are dominated by tensile residual stresses from thermal expansion mismatch (**Fig 3**) in agreement with previous work [14]. Based on the thermal strain relation, the stresses due to a CTE mismatch would be around 70 MPa which is partly due to the phase transformation from cubic $MAPbI_3$ to tetragonal $MAPbI_3$ that occurs at 55°C [13]. Additives lead to slower and more uniform crystallization confirmed by the longer observed conversion time; however, the stress also increases with additive concentration for both starch and gellan gum. This is likely due in part to the higher temperature of attachment for the films that converted more slowly with additives. We also fabricated $MAPbI_3$ films with the same recipe in a nitrogen-controlled glove box to isolate any contributions from moisture in the ambient environment and observed similar values. (**Fig. 3b**).

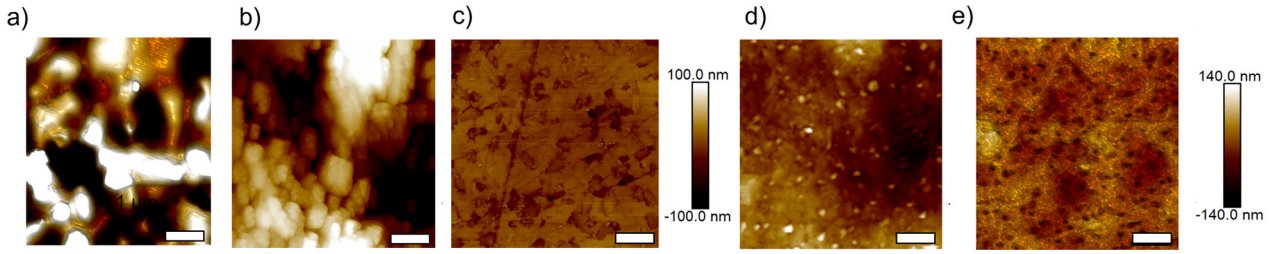

Fig 4 AFM 3D images for the (a) blade coated control and perovskite thin films with (b) 0.3 wt% gellan gum, and (c) 1.1 wt% gellan gum (d) 5wt% corn starch, (e) 10 wt% corn starch. The white scale bar represents 1 μm. The height for (a-c) is -100 nm to 100 nm and for (d-e) is -140 nm to 140 nm.

Blade coated $MAPbI_3$ films showed a different trend, where compression was induced above a certain threshold additive concentration. For gellan gum, we used a smaller amount because lower additive concentrations achieve comparably high viscosity compared to starch, as shown in Figure S2. Compressive stresses were observed past 1wt% of gellan gum. while the films with starch showed compressive stresses for 2.5wt% addition and above in the precursor solution (Fig. 3 (c)-(d)). The change in stress states when spin coating to blade coating can be explained by the solvent removal rate and the subsequent crystallization of the perovskite layer. The solvent evaporation and retention for solution-based precursors defines the structural differences in thin films and they are closely linked to the deposition technique [35]. A slower rate of solvent removal and lesser overall evaporated solvent was seen in spin coated films [35].

The morphology also changed significantly for films under tension to compression, which is indicative of intrinsic sources of stress based on perovskite microstructure. The AFM image in **Fig 4 (a)** for the blade coated control perovskite solution shows poor coverage and small grains with an average roughness of 100.6 nm. As the gellan gum concentration increased to 0.3wt%, there was an improvement in coverage, as seen in **Fig. 4 (b)**, but the films were still rough (average roughness of 46.6 nm) with nanoscale grains. Beyond 1wt% when the film achieves compressive stress, the morphology improves to a smoother and uniform film with an average roughness of 9.6 nm (**Fig. 4 (c)).** A similar trend was observed with starch

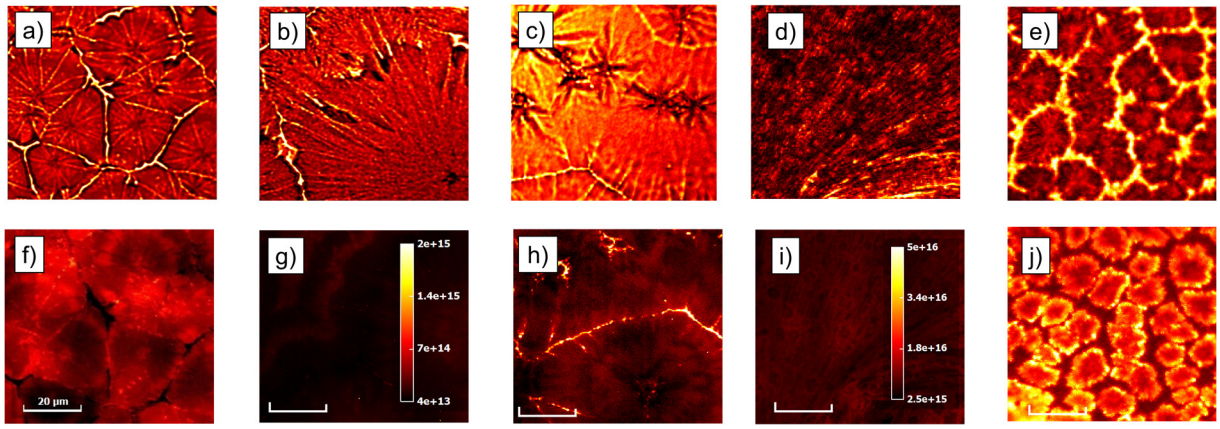

Fig 5 Hyperspectral photoluminescence images show the optical transmission images for perovskite thin films with (a) no additive, (b) 0.3 wt% gellan gum (c) 0.56 wt% gellan gum (d) 2.5 wt% starch, (e) 5 wt% starch, and photoluminescence images for (f) no additive, (g) 0.3 wt% gellan gum (h) 0.56 wt% gellan gum, (i) 2.5 wt% starch, (j) 5 wt% starch. The scale bars in (f), (g), and (h) are the same. The scale bars in (i) and (j) are the same.

where the films under compression were more uniform and of higher quality where the average roughness reduced to 12 nm. (**Fig.4(e)**).

The addition of polymers not only affects the crystallization but also changes the coordination of the solvent and precursor altering the final properties of the perovskite layer. The solvent-intermediated complexes nucleate and texture differently during drying of the solvent because of the local environment and the intermediate adduct phase [36], an effect which could explain the differing microstructure seen in our final films.

The optoelectronic properties of $MAPbI_3$ films were also studied as a function of film stress. In **Fig. 5**, the top row shows the transmission images depicting the microstructure of the perovskite films compared to hyperspectral photoluminescence maps in the bottom row averaged over 400-1000 nm. The control film in **Fig. 5 (f)** showed some non-luminescent grain boundaries, indicating that there were non-radiative recombination centers in these areas [37], [38]. Highly tensile films with a low additive concentration showed reduced luminescence at both the boundaries and the bulk of the film (**Fig. 5 (g)**), which could be attributed to an increase in non-radiative recombination across the film. However, for a compressive sample, the grain boundaries were luminescing at a higher intensity, **Fig. 5 (h)**.

We also studied the effects on starch and **Fig. 5 (j)** shows the compressive sample with 5wt% starch which also showed luminescent grain boundaries. Darker regions are evident in the higher starch concentration, but that can be ascribed to thinner coverage between the grains from the optical transmission data in **Fig 5 (e)**. The tensile film with starch in **Fig. 5 (i)** also shows a comparably lower PL intensity to the compressive

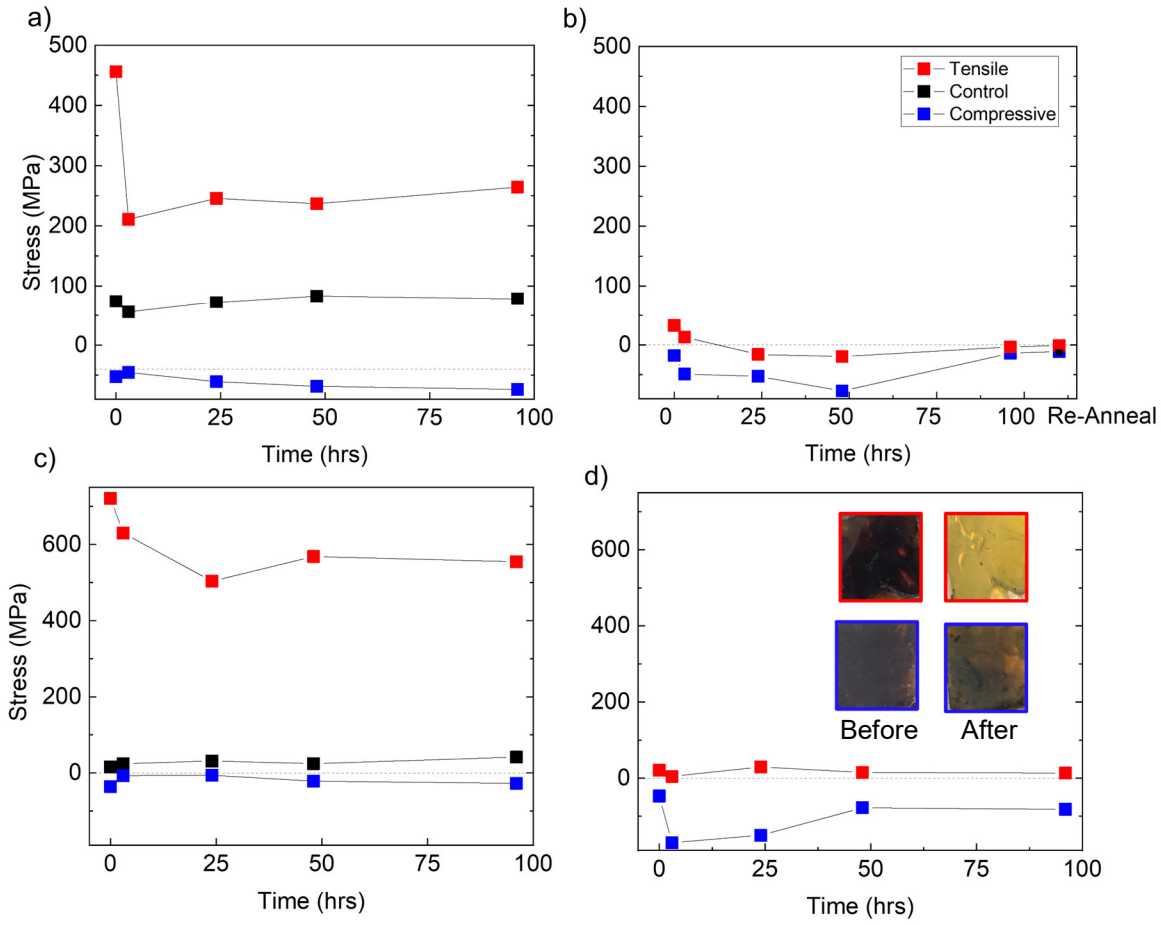

Fig 6 Stress measurements from aging the samples at 85% relative humidity for 100 hours using a control, tensile and compressive $MAPbI_3$ film with (a) gellan gum (b) corn starch. The samples were also kept at 85°C with the same conditions with (c) gellan gum (d) corn starch. The insets in 6 (d) show the tensile (red) and compressive (blue) films before (left) and after (right) 100 hours of aging.

film. This data indicates that compressive stresses could possibly be assisting with absorbance and may reduce recombination losses. The additives may not only be slowing down crystallization but also concentrating at the boundaries to relieve the intrinsic stress associated with them. Residual film stresses could play a key role in perovskite optoelectronic properties.

Given the strong link between residual stress and degradation [39]–[41], we assessed the stability of perovskite films with different residual stress states. Bare perovskite films on silicon and glass were stress engineered using additives to either be tensile or compressive and aged under either high heat or humidity conditions (85°C or 85% relative humidity). A control $MAPbI_3$ film spin coated without additives was also added as a reference under 85% relative humidity. The samples were periodically removed, and the stress was remeasured in ambient conditions (22°C and 40% RH). **Fig. 6 (a)** shows the highly tensile samples experienced stress relaxation quickly in the humid environment due to moisture induced degradation. This effect was not observed for samples with compressive stress, which also did not experience visible degradation during the 100-hour exposure. We performed XRD measurements (**Fig. S3**) on these films to verify degradation and the tensile sample had PbI_2 peaks after the aging experiment, whereas the compressive sample had lower intensity PbI_2 peaks and still had $MAPbI_3$ in the film. This confirms that perovskites are more structurally stable when exposed to environmental conditions while in compression.

Samples were reannealed to ensure that trapped moisture was not the cause of the relaxation, and there was no change observed in the stress (**Fig. 6 (b)**). Therefore, residual moisture is not the explanation for the stress reduction.

A similar experiment was conducted for thermal stability at 85°C under vacuum to monitor the changes in stress under thermal aging. Once again, stress relaxation was observed for the highly tensile sample with gum in **Fig. 6 (c)**. The improvement in stability was visually apparent since the tensile films turned completely yellow after being aged for 100 hours while the compressive one remained largely in the black photoactive phase. The samples with additives took longer to visibly degrade as seen in the insets in **Fig. 6 (d)** which also points towards their improved stability. The tensile stress was therefore relaxing as the film degraded due to the strained bonds likely enabled the methylammonium cation to diffuse out, whereas a compressive stress showed better stability and unchanging stress under heat, similar to the effect observed with aging in high humidity.

A thermal cycling experiment was also conducted for a tensile and compressive sample to monitor the perovskite films as the temperature changes between -40 to 85°C. The experiment ran for 200 cycles and the results supported what was observed under high heat and humidity conditions. **Fig. 7** shows the tensile sample relaxed by 180 MPa and turned completely yellow. However, the compressive sample was stable both in terms of its appearance and film stress. A spin coated $MAPbI_3$ film without additives (with tensile residual stress) was kept as the control sample. In all three aging conditions, films with residual tensile stress degraded significantly faster. The degradation also corresponded to stress relaxation in the perovskite film as the phase changed, marking the first time for which changes in stress have been directly mapped to stability. Stress relaxation has been observed in many other material systems (*i.e.,* polymers and metals) when exposed to tensile stress. Perovskites therefore act similarly, and despite their brittle nature, share in this property. The exact mechanism requires further investigation, and we hypothesize that diffusion along grain boundaries and dislocation motion could be at play.

[16]

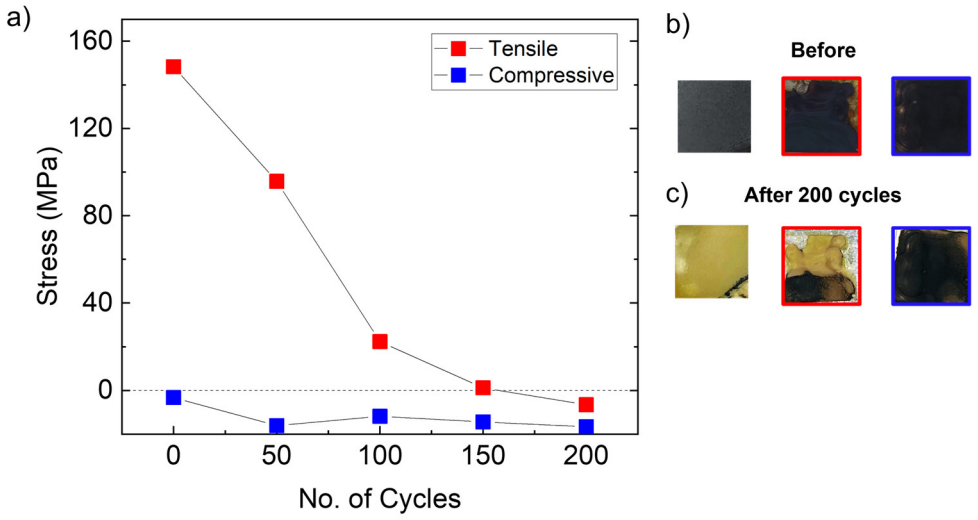

Fig 7 (a) A tensile and compressive $MAPbI_3$ film as it is thermally cycled from -40 to 85°C for 200 cycles. The photographs on the right show the samples (b) before and (c) after 200 cycles for the (L to R) control, tensile and compressive films.

III. Conclusion and Outlook

Our findings suggest that blade coating assisted with the polymer induces a desirable compression in thin film perovskites which can be attributed to a more balanced crystal nucleation and growth regime.

Residual film stresses can be either related to thermal expansion mismatch between the film and substrate (thermal effects) or evolve either during perovskite crystallization (intrinsic effects). With the help of biopolymer additives and a scalable processing technique it is possible to introduce a compressive intrinsic stress. The compressive stress improves film quality, optoelectronic properties, and operational stability of the perovskite absorber layer. Films under compressive stress demonstrate a better resistance to high heat and humidity as well as thermal cycling. We have shown compressive film stresses desirable for enhanced operational stability of the perovskite layer with increases in photon flux across the film. The polymer additives also increase the fracture resistance of the perovskite film, making it less likely to crack or delaminate.

Most notably, this work shows a systematic change in perovskite film stress under operational conditions, particularly for films with residual tensile stresses. For the first time, stress relaxation is observed in perovskites and mapped to film degradation. By understanding the mechanisms of stress-related degradation and controlling them through processing strategies, we hope to enable robust and manufacturable perovskite solar cells in single-junction or multi-junction architectures.

Author Contributions

The manuscript was written through contributions of all authors. All authors have given approval to the final version of the manuscript.

References

[1] J. Y. Kim, J.-W. Lee, H. S. Jung, H. Shin, and N.-G. Park, "High-Efficiency Perovskite Solar Cells," *Chem Rev*, vol. 120, no. 15, pp. 7867–7918, Aug. 2020, doi: 10.1021/acs.chemrev.0c00107.

[2] J. J. Yoo, S. S. Shin, and J. Seo, "Toward Efficient Perovskite Solar Cells: Progress, Strategies, and Perspectives," *ACS Energy Lett*, vol. 7, no. 6, pp. 2084–2091, Jun. 2022, doi: 10.1021/acsenergylett.2c00592.

[3] R. Sharma, A. Sharma, S. Agarwal, and M. S. Dhaka, "Stability and efficiency issues, solutions and advancements in perovskite solar cells: A review," *Solar Energy*, vol. 244, pp. 516–535, Sep. 2022, doi: 10.1016/J.SOLENER.2022.08.001.

[4] G. Kim, H. Min, K. S. Lee, D. Y. Lee, S. M. Yoon, and S. Il Seok, "Impact of strain relaxation on performance of α-formamidinium lead iodide perovskite solar cells," *Science (1979)*, vol. 370, no. 6512, pp. 108–112, Oct. 2020, doi: 10.1126/science.abc4417.

[5] D. Ramirez, "Stable Hybrid Perovskite Materials for Photovoltaics Under Real-World Conditions," *Materials Today Electronics*, vol. 4, p. 100038, 2023, doi: 10.1016/j.mtelec.2023.100038.

[6] P. Bhatt *et al.*, "A review on computational modeling of instability and degradation issues of halide perovskite photovoltaic materials," *Wiley Interdiscip Rev Comput Mol Sci*, p. e1677, Jun. 2023, doi: 10.1002/WCMS.1677.

[7] D. Wang, M. Wright, N. K. Elumalai, and A. Uddin, “Stability of perovskite solar cells,” *Solar Energy Materials and Solar Cells*, vol. 147, pp. 255–275, Apr. 2016, doi: 10.1016/J.SOLMAT.2015.12.025.

[8] T. M. Koh, K. Thirumal, H. Sen Soo, and N. Mathews, “Multidimensional Perovskites: A Mixed Cation Approach Towards Ambient Stable and Tunable Perovskite Photovoltaics,” *ChemSusChem*, vol. 9, no. 18, pp. 2541–2558, Sep. 2016, doi: 10.1002/CSSC.201601025.

[9] Z. Dai *et al.*, “The mechanical behavior of metal-halide perovskites: Elasticity, plasticity, fracture, and creep,” *Scr Mater*, vol. 223, Jan. 2023, doi: 10.1016/j.scriptamat.2022.115064.

[10] A. G. Evans, M. D. Drory, and M. S. Hu, “The cracking and decohesion of thin films,” *J Mater Res*, vol. 3, no. 5, pp. 1043–1049, 1988, doi: 10.1557/JMR.1988.1043.

[11] M. Dailey, Y. Li, and A. D. Printz, “Residual Film Stresses in Perovskite Solar Cells: Origins, Effects, and Mitigation Strategies,” *ACS Omega*, vol. 6, no. 45. American Chemical Society, pp. 30214–30223, Nov. 16, 2021. doi: 10.1021/acsomega.1c04814.

[12] N. Rolston *et al.*, “Engineering Stress in Perovskite Solar Cells to Improve Stability,” *Adv Energy Mater*, vol. 8, no. 29, Oct. 2018, doi: 10.1002/aenm.201802139.

[13] L. E. Mundt, L. T. Schelhas, and K. H. Stone, “Accurately Quantifying Stress during Metal Halide Perovskite Thin Film Formation,” *ACS Appl Mater Interfaces*, vol. 14, no. 24, pp. 27791–27798, Jun. 2022, doi: 10.1021/acsami.2c01654.

[14] K. A. Bush *et al.*, “Controlling Thin-Film Stress and Wrinkling during Perovskite Film Formation,” *ACS Energy Lett*, vol. 3, no. 6, pp. 1225–1232, Jun. 2018, doi: 10.1021/acsenergylett.8b00544.

[15] I. Sacligil, C. W. Barney, A. J. Crosby, and G. N. Tew, “Bond strength regime dictates stress relaxation behavior,” *Soft Matter*, vol. 18, no. 26, pp. 4937–4943, 2022, doi: 10.1039/D2SM00499B.

[16] N. Obaid, M. Kortschot, and M. Sain, “Understanding the Stress Relaxation Behavior of Polymers Reinforced with Short Elastic Fibers,” *Materials*, vol. 10, no. 5, p. 472, Apr. 2017, doi: 10.3390/ma10050472.

[17] J. Zhao *et al.*, “Strained hybrid perovskite thin films and their impact on the intrinsic stability of perovskite solar cells,” 2017. [Online]. Available: https://www.science.org

[18] S. K. Yadavalli, Z. Dai, H. Zhou, Y. Zhou, and N. P. Padture, “Facile healing of cracks in organic–inorganic halide perovskite thin films,” *Acta Mater*, vol. 187, pp. 112–121, Apr. 2020, doi: 10.1016/j.actamat.2020.01.040.

[19] A. Giuri *et al.*, “Robust, High-Performing Maize–Perovskite-Based Solar Cells with Improved Stability,” *ACS Appl Energy Mater*, vol. 4, no. 10, pp. 11194–11203, Oct. 2021, doi: 10.1021/acsaem.1c02058.

[20] M. F. Doerner and W. D. Nix, “Stresses and deformation processes in thin films on substrates,” *Critical Reviews in Solid State and Materials Sciences*, vol. 14, no. 3, pp. 225–268, Jan. 1988, doi: 10.1080/10408438808243734.

[21] "Thermal Expansion - Linear Expansion Coefficients." https://www.engineeringtoolbox.com/linear-expansion-coefficients-d_95.html (accessed Jun. 26, 2023).

[22] T.-H. Han *et al.*, "Perovskite-polymer composite cross-linker approach for highly-stable and efficient perovskite solar cells," *Nat Commun*, vol. 10, no. 1, p. 520, Jan. 2019, doi: 10.1038/s41467-019-08455-z.

[23] H. Wang *et al.*, "Interfacial Residual Stress Relaxation in Perovskite Solar Cells with Improved Stability," *Advanced Materials*, vol. 31, no. 48, p. 1904408, Nov. 2019, doi: https://doi.org/10.1002/adma.201904408.

[24] E. Johlin *et al.*, "Structural origins of intrinsic stress in amorphous silicon thin films," *Phys Rev B*, vol. 85, no. 7, p. 075202, Feb. 2012, doi: 10.1103/PhysRevB.85.075202.

[25] L. Wang *et al.*, "Strain Modulation for Light-Stable n–i–p Perovskite/Silicon Tandem Solar Cells," *Advanced Materials*, vol. 34, no. 26, p. 2201315, Jul. 2022, doi: 10.1002/ADMA.202201315.

[26] C. Shi *et al.*, "Molecular Hinges Stabilize Formamidinium-Based Perovskite Solar Cells with Compressive Strain," *Adv Funct Mater*, vol. 32, no. 28, p. 2201193, Jul. 2022, doi: 10.1002/ADFM.202201193.

[27] C.-Y. Chang *et al.*, "Tuning Perovskite Morphology by Polymer Additive for High Efficiency Solar Cell," *ACS Appl Mater Interfaces*, vol. 7, no. 8, pp. 4955–4961, 2015, doi: 10.1021/acsami.5b00052.

[28] D. Bi *et al.*, "Polymer-templated nucleation and crystal growth of perovskite films for solar cells with efficiency greater than 21%," *Nat Energy*, vol. 1, no. 10, p. 16142, 2016, doi: 10.1038/nenergy.2016.142.

[29] G. Yuan *et al.*, "Inhibited Crack Development by Compressive Strain in Perovskite Solar Cells with Improved Mechanical Stability," *Advanced Materials*, vol. 35, no. 17, p. 2211257, Apr. 2023, doi: 10.1002/ADMA.202211257.

[30] F. Bisconti *et al.*, "Polymer-Assisted Single-Step Slot-Die Coating of Flexible Perovskite Solar Cells at Mild Temperature from Dimethyl Sulfoxide," *Chempluschem*, vol. 86, no. 10, pp. 1442–1450, Oct. 2021, doi: 10.1002/CPLU.202100251.

[31] A. Giuri *et al.*, "Polymeric rheology modifier allows single-step coating of perovskite ink for highly efficient and stable solar cells," *Nano Energy*, vol. 54, pp. 400–408, Dec. 2018, doi: 10.1016/j.nanoen.2018.10.039.

[32] F. Bisconti *et al.*, "One-step polymer assisted roll-to-roll gravure-printed perovskite solar cells without using anti-solvent bathing," *Cell Rep Phys Sci*, vol. 2, no. 11, p. 100639, Nov. 2021, doi: 10.1016/j.xcrp.2021.100639.

[33] A. A. Petrov *et al.*, "Crystal Structure of DMF-Intermediate Phases Uncovers the Link Between $CH_3NH_3PbI_3$ Morphology and Precursor Stoichiometry," *The Journal of Physical Chemistry C*, vol. 121, no. 38, pp. 20739–20743, Sep. 2017, doi: 10.1021/acs.jpcc.7b08468.

[34] J. Yang *et al.*, "A Review on Improving the Quality of Perovskite Films in Perovskite Solar Cells via the Weak Forces Induced by Additives," *Applied Sciences*, vol. 9, no. 20, p. 4393, Oct. 2019, doi: 10.3390/app9204393.

[35] Y. Zhong *et al.*, "Blade-Coated Hybrid Perovskite Solar Cells with Efficiency > 17%: An In Situ Investigation," *ACS Energy Lett*, vol. 3, no. 5, pp. 1078–1085, May 2018, doi: 10.1021/acsenergylett.8b00428.

[36] S. Il Seok, M. Grätzel, N.-G. Park, S. I. Seok, M. Grätzel, and -G N Park, "Methodologies toward Highly Efficient Perovskite Solar Cells," *Small*, vol. 14, no. 20, p. 1704177, May 2018, doi: 10.1002/SMLL.201704177.

[37] J. Gu *et al.*, "Correlating Photophysical Properties with Stereochemical Expression of 6s2 Lone Pairs in Two-dimensional Lead Halide Perovskites," *Angewandte Chemie*, p. e202304515, Jun. 2023, doi: 10.1002/ANGE.202304515.

[38] M. T. Khan, "Unraveling the impact of graphene nanostructures passivation on the electrical properties of the perovskite solar cell," *Mater Sci Semicond Process*, vol. 153, p. 107172, Jan. 2023, doi: 10.1016/J.MSSP.2022.107172.

[39] X. Liu *et al.*, "Epitaxial 2D PbS Nanosheet-Formamidinium Lead Triiodide Heterostructure Enabling High-Performance Perovskite Solar Cells," *Adv Funct Mater*, p. 2304140, 2023, doi: 10.1002/ADFM.202304140.

[40] S. Chen *et al.*, "Atomic-Scale Polarization and Strain at the Surface of Lead Halide Perovskite Nanocrystals," *Nano Lett*, Jun. 2023, doi: 10.1021/ACS.NANOLETT.3C01189.

[41] S.-Y. Ju, W. I. Lee, and H.-S. Kim, "Enhanced Phase Stability of Compressive Strain-Induced Perovskite Crystals," *ACS Appl Mater Interfaces*, vol. 14, no. 35, pp. 39996–40004, Sep. 2022, doi: 10.1021/acsami.2c10450.

Supplementary Information

Materials and Methods

Methylammonium iodide >99.99% was purchased from Greatcell Solar, Lead (II) iodide 99.99% for perovskite precursor was purchased from TCI, Methyl sulfoxide ≥ 99% was purchased from Sigma Aldrich. Gellan gum and Corn starch powders were purchased from Alfa Aesar.

To prepare the $CH_3NH_3PbI_3$ solution, we dissolved 230.5 mg of PbI_2 and 59.5 mg of CH3NH3I in 1 ml of DMSO to make a 0.5M stock solution in the glovebox. The films with gellan gum and corn starch were prepared by adding the additives by weight percent of the powders in the $CH_3NH_3PbI_3$ precursor. For starch we used concentrations of 2.5-20 wt% while for gellan gum we used 0.3 to 2.25 wt%. The solution was stirred at 80°C for three hours. Films prepared by spin coating were spun at 4000 rpm for 30 seconds while for blade coating, we coated at a speed of 10 mm/s. All films were annealed at 100°C for 20 minutes.

Hyperspectral photoluminescence measurements were conducted using the Photon Etc IMA microscope with a magnification of 50X and field of view 134 μm by 181 μm. The samples were excited at 532 nm

with an exposure time of 3 seconds. The hyperspectral images were taken between 700 to 875 nm with increment steps of 2 nm under absolute calibration.

Bruker Multimode 8 Atomic Force Microscope was used to image the surface of our samples. The images were recorded at a 5μm x 5 μm resolution with a scan rate of 1 Hz and 256 lines/sample. The Olympus microscope DSX-1000 was used to verify the morphology of the sample using the transillumination settings.

The thickness of the films was measured using the Tencor P-16 contact profilometer. The scan length was set at 443 μm with a speed of 2 μm/s and a scan rate of 50 Hz. The stylus applies a force of 5mg on the sample to measure small surface variations.

The samples were thermally cycled from -40 to 85°C in the Thermotron Model SM-8-8200 Environmental Test Chamber. The samples stayed at the extremes of -40 and 85°C for a total of 10 minutes and the temperature was ramped at 4°C per minute.

For the purpose of measuring stress, we used the Tencor FLX-265P film stress measurement system. It is a simple, quick and non-destructive technique that uses a laser to measure the change in curvature of the substrate. The deflection of the substrate is measured by the reflected laser intensity before and after the perovskite film deposition. The system program calculates the film stress using Stoney's equation **(Equation 3)** and requires the thickness of the film, substrate, Young's Modulus of the substrate to proceed.

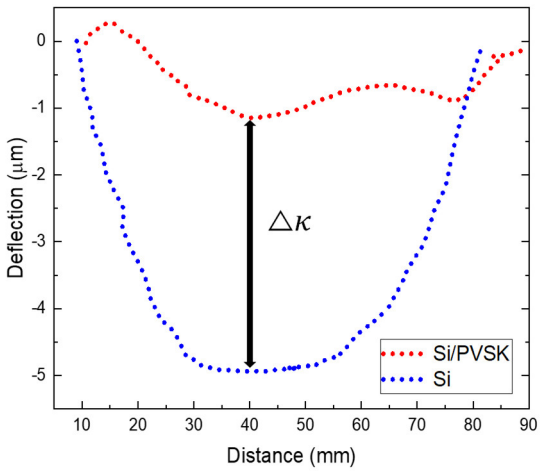

Fig S1 The change in curvature, $\triangle\kappa$, as measured by the Tenor FLX-265P.

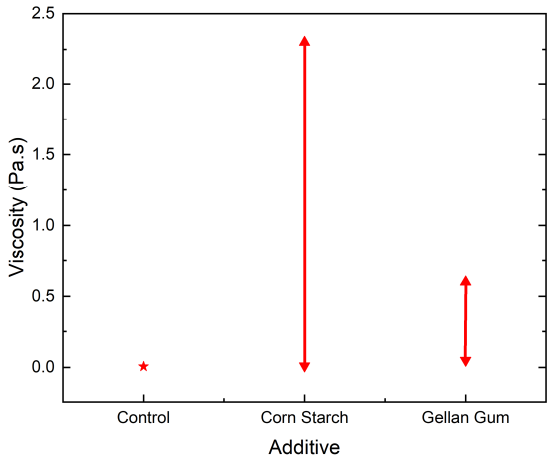

Fig S2 Viscosity ranges for MAPbI3 control solution and with additives corn starch from 2.5-20 wt% and gellan gum 0.5 to 2.5 wt%

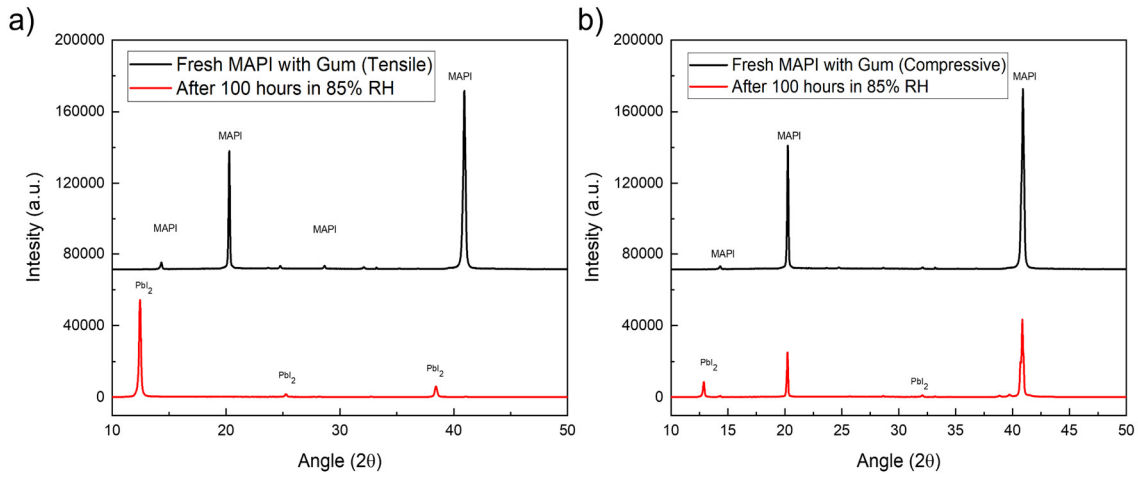

Fig S3 XRD data for (a) the tensile sample with 0.5wt% gum and the (b) the compressive sample with 1.1wt% gum fresh and after 100 hours of aging under 85% relative humidity.

$MAPbI_3$ Concentration	**Gellan Gum Concentration**	**Average Thickness of the Film**
28 wt%	0.3 wt%	150 nm
28 wt%	0.56 wt%	200 nm
28 wt%	1.1 wt%	500 nm
28 wt%	2.25 wt%	Too viscous to blade coat

Table S1: Concentrations for MAPbI3 and gellan gum additive used s and thicknesses for blade-coated samples.

$MAPbI_3$ Concentration	**Gellan Gum Concentration**	**Average Thickness of the Film**
28 wt%	2.5 wt%	120 nm
28 wt%	5 wt%	420 nm
28 wt%	10 wt%	490 nm
28 wt%	20 wt%	560 nm

Table S2: Concentrations for MAPbI3 and gellan gum additive used and thicknesses for blade-coated sampless.